Synthesis and analysis of linear and nonlinear acoustical vortices

Régis Marchiano*
Laboratoire de Modélisation en Mécanique (UMR CNRS 7607), Université Pierre et Marie Curie 4, place Jussieu, 75252 Paris Cedex 05, France

Jean-Louis Thomas
Institut des NanoSciences de Paris (UMR CNRS 7588), Université Pierre et Marie Curie 140, rue de Lourmel, 75015 Paris, France
(Received 15 March 2005; published 30 June 2005)

Acoustical screw dislocations are synthesized in various configurations with a versatile experimental setup. The experimental setup is based on the inverse filter technique and allows one to synthesize one or more acoustical vortices with a chosen width, position, and topological charge. An interesting feature of this experimental facility to study screw dislocation behavior is the direct measurement in amplitude and phase. This characteristic is used to develop an original method of decomposition of an acoustical vortex field in order to analyze the acoustical vortices. Moreover, the behaviors of two acoustical vortices of the same or opposite charge have been studied experimentally and compared to theoretical laws.

DOI: 10.1103/PhysRevE.71.066616 PACS number(s): 43.35.+d, 43.25.+y, 43.20.+g

I. INTRODUCTION

Phase singularities are important features of a wave field because they are generic and structurally stable [1]. Physically, this means, respectively, that they are naturally produced in a wave field, and that a weak perturbation of the field does not eliminate them. Even though the first work about these kinds of structure was realized by Whewell in 1833 [2] about the amphidromic point in the North Sea, the nature of these structures was analyzed in detail only recently by Nye and Berry in 1974 [3]. In that paper, they introduced the concept of phase singularity in the wave theory and classified the three kinds of phase singularities: edge dislocation, screw dislocation, and mixed type screw-edge dislocation.

Since the beginning of the 1990s, there has been a wide interest in these structures particularly in optics. A different branch of optics has risen up with what is called singular optics [4]. Screw dislocations took up a particular place in this field of optics and are also known as optical vortices. Such a structure possesses one point, where the phase is undetermined, and around which the phase is winding. A schematic representation of the phase of such a structure is depicted in Fig. 1: the black line represents the axis along which the phase is winding. The number of jumps of 2π achieved by the phase on a close contour around that point is called the topological charge, denoted l ($|l|=1$ in Fig. 1) and the sense of the winding gives the sign of the topological charge: positive for counterclockwise and negative for clockwise [5] ($l=-1$ in Fig. 1). At that point, the amplitude of the wave field is null and it forms a dark core because of destructive interference: the fields at two points symetric in relation to the center of the beam are dephased by π. Besides the structural stability and genericity, optical vortices have many interesting properties. Indeed, they carry an angular momentum [6], they exhibited self-reconstruction ability [7], and moreover there exist analogies with hydrodynamic vortices and quantum mechanics.

Suprisingly, there are only a small number of studies in acoustics for which similar properties are expected. Hefner and Marston [8] demonstrated the possibility of generating single acoustical vortices of charge 1 and they proposed to use them for underwater alignment thanks to the very narrow zero amplitude associated with them. Recently, Gspan *et al.* [9] showed that these structures could be produced by optoacoustic generation. In a previous paper, Thomas and Marchiano [10] demonstrated that the pseudo-angular-momentum and the pseudoenergy of an acoustical vortex are related to its topological charge. This result can be interpreted in an isotropic and inviscid medium as a law of conservation of the topological charge. This result generalizes a previous result valid for electromagnetic waves in the vacuum [6] to mechanical waves and optical waves in dielectric media. Moreover, it was extended to the case of weak nonlinear acoustics for which it predicts a linear increase of the topological charge with nonlinear generation of harmonics. This phenomenon has been confirmed experimentally.

In this paper, a versatile experimental setup allowing one to synthesize various configurations with acoustical vortices is proposed.

First, the synthesis of single vortices of charge -1 and -3 is presented in detail. Then the nature of these beams is analyzed precisely through a modal decomposition of the experimental fields in terms of Gauss-Laguerre modes. Finally, the dynamics of the interaction of two vortices of the same and opposite charges is presented and compared favorably to theoretical laws.

II. EXPERIMENTAL SETUP

Screw dislocations exist naturally in wave fields; this is related to the concept of genericity. The amphidromic point [2] is one of the examples of natural screw dislocations for

*Electronic address: marchi@lmm.jussieu.fr

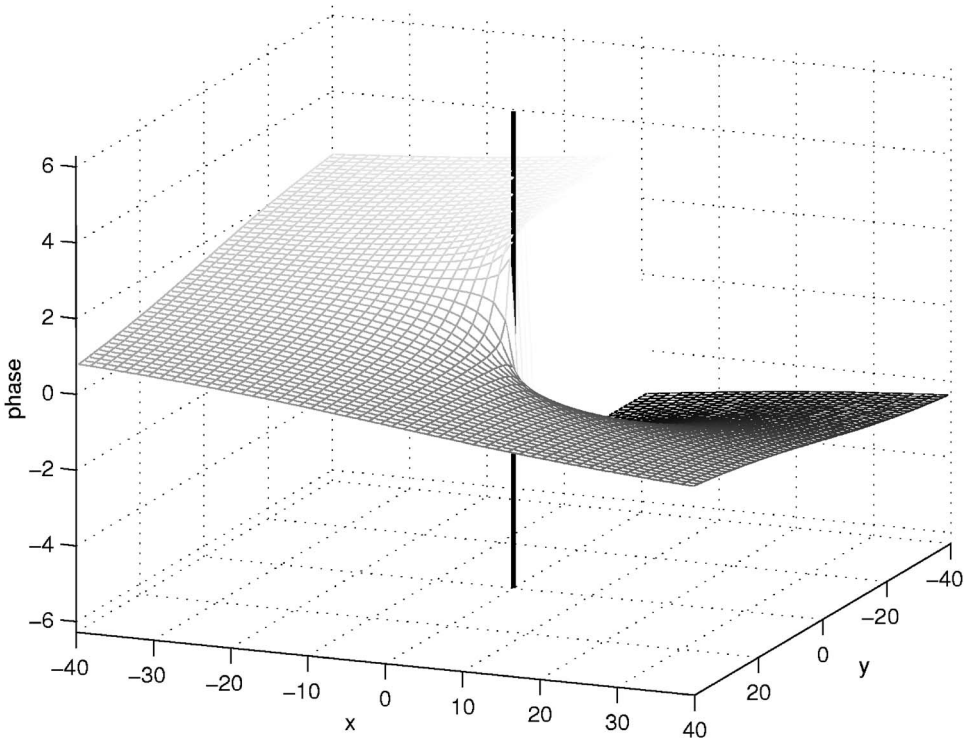

FIG. 1. Schematic representation of a clockwise screw dislocation ($l=1$).

gravity waves, but there exist other examples. Let us cite the screw dislocations produced by reflection on a rough surface [3] or observed in speckles [11]. But to study accurately their structures, it is more convenient to synthesize screw dislocations with well-defined width, position, and topological charge. Several methods have been proposed especially in optics. The most used method consists in synthesizing vortices thanks to holograms. The holograms are generated with the help of a computer and there exist different types of holograms [12]. Optical vortices can be created by conversion of a Hermit- Gaussian mode into a Gauss-Laguerre mode also [13]. Another way of synthesizing is to use a suitable mask for the amplitude or the phase [14]. Recently, methods based on spatial light modulator techniques were proposed [15]. In acoustics, Hefner and Marston [8] proposed two methods to create acoustical screw dislocations of charge 1. The first one consists in a transducer with a helical shape and the second one in an array of four transducers which send signals with a $\pi/2$ difference of phase. Recently, Gspan *et al.* [9] suggested proceeding by optoacoustic generation. But so far all these techniques have only produced simple acoustical vortices of charge 1.

Here, we propose to use the inverse filter technique [16] to synthesize one or more vortices with a chosen topological charge. The inverse filter technique is a powerful method of linear wave field synthesis. It is based on knowledge of the medium of propagation between the acoustical sources and the points where the field should be synthesized, namely, the control points. Once the propagation operator is experimentally recorded, an appropriate numerical treatment is applied to compute the signals that the transducers have to emit to synthesize the desired field at the control point. This method ensures that the synthesized field is then the closest one feasible for a given configuration. It is a very versatile method, because once the operator is acquired and numerically treated, the determination of the signal to emit is very quick. That is why it is reasonable to envisage a real time control of the vortex properties in the future, but it is not the key point of this paper.

The experimental setup is made of an array of 61 piezoelectric transducers immersed in water (Fig. 2). The central frequency of the transducers is 1 MHz; the corresponding wavelength is then $\lambda=1.5$ mm. Each transducer is a circle of 11 mm diameter separated from the other transducers by a 1 mm space. The transducers are distributed on a regular hexagon 100 mm high. The amplitude and the phase of each of them can be driven independently thanks to electronic amplifiers (Lecoeur Electronique). The acoustical field is recorded by a hydrophone, measuring the instantaneous amplitude, associated with a digital oscilloscope. Step by step motors authorize the displacement of the hydrophone in the three directions of space. We define a control plane located 500 mm away from the array of transducers where the acoustical vortices will be created. In this plane the field is sampled with 2916 points regularly set on a square grid of 80×80 mm^2 with a spatial step of 1.5 mm. The propagation operator is recorded between these points and the array of transducers. The array of transducers, the digital oscilloscope, and the step by step motors are linked up to a PC which controls the whole experiment and in which the data are stored.

III. EXPERIMENTAL RESULTS

A. Synthesis of single acoustical vortices

To synthesize acoustical vortices, we choose to use the Gauss-Laguerre (GL) beams as pattern in the control plane.

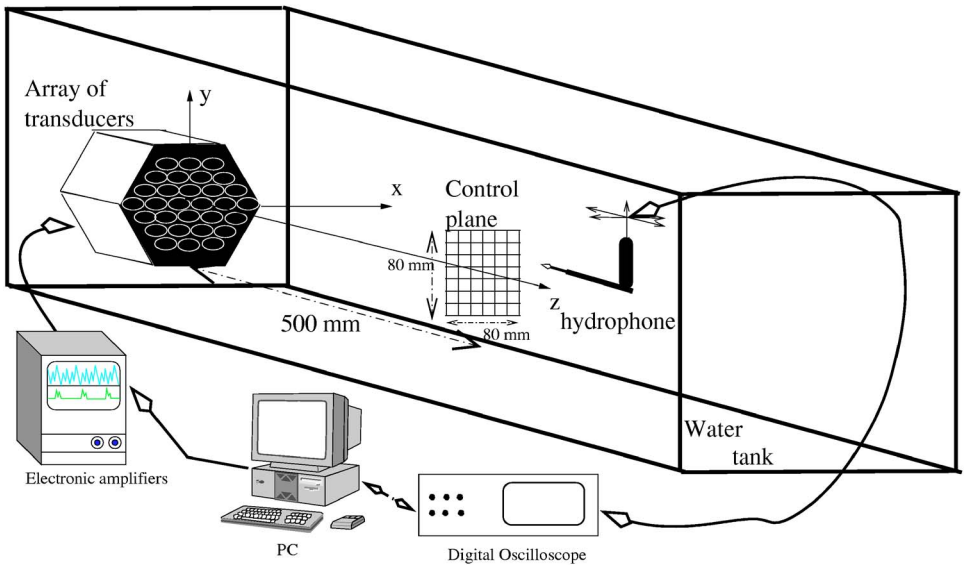

FIG. 2. Experimental setup.

Indeed, these beams are known to carry screw dislocations [17] and are solutions of the paraxial propagation equation.

Let us consider the cylindrical coordinates system (O,r,ϕ,z), with O the origin attached to the center of the array of transducers, z the direction of propagation normal to the array of transducers, and (r,ϕ) the cylindrical coordinates in a transverse plane [the plane denoted (x,y) in the sketch of the experimental setup Fig. 2]. The pressure associated with a GL beam at point (r,ϕ) in a plane parallel to the array of transducers and located at a distance z from it can be expressed [17]

$$P(r,\phi,z,t) = p_{n,l}(r,\phi,z)\exp[i(kz-\omega t)]. \tag{1}$$

The term $p_{n,l}(r,\phi,z)$ describes the pressure distribution in planes transverse to the direction of propagation:

$$p_{n,l}(r,\phi,z) = G(r,z)A_{n,l}(r,z)\Phi_l(\phi)\Psi_n(z). \tag{2}$$

The different terms in the last expression describe, respectively, the Gaussian envelope of the beam, the amplitude structure near the dark core, the phase structure of the beam, and the Gouy phase.

The Gaussian envelope of the beam is:

$$G(r,z) = \frac{D}{(1+z^2/z_R^2)^{1/2}}\exp\left(\frac{r^2}{w^2(z)}\right)\exp\left(-i\frac{kr^2z}{2(z^2+z_R^2)}\right), \tag{3}$$

where D is a constant for the normalization, $z_R = kw_0^2/2$ is the Rayleigh distance (w_0 being the width of the beam at $z=0$ and k the wave number), and $w(z) = w_0[1+(z/z_R)^2]^{1/2}$ describes the evolution of the size of the Gaussian beam during the propagation.

The amplitude structure near the center of the beam is given by

$$A_{n,l}(r,z) = \left(\frac{r\sqrt{2}}{w(z)}\right)^{|l|} L^{|l|}_{(n-|l|)/2}\left(\frac{2r^2}{w^2(z)}\right), \tag{4}$$

where $L^{|l|}_{(n-|l|)/2}$ denotes the generalized Laguerre polynomials [18] with $n=|l|,|l|+2,|l|+4,\ldots$ the radial index and l the topological charge.

The helical structure of the phase of the beam is due to the term

$$\Phi_l(\phi) = \exp(il\phi). \tag{5}$$

An additional phase term is required to take into account the Gouy phase:

$$\Psi_n(z) = \exp[-i(n+1)\psi(z)], \tag{6}$$

where $\psi(z) = \arctan z/z_R$.

1. Single vortex of charge −1

To synthesize a single vortex of charge −1 in the control plane, the GL mode $p_{1,-1}(r,\phi,0)$ with a width of $w_0 = 10\lambda$ is taken as pattern. The rms amplitude and the phase of this pattern are given in Fig. 3, respectively, on the left and on the right. The signals to be emitted by the array of transducers are calculated by the inverse filter technique from the propagation operator and the pattern. They are emitted at low amplitude to ensure the linearity of the propagation. The pressure field in the control plane is then recorded: at each point of the control plane, the instantaneous amplitude is measured. The instantaneous amplitude is given in Fig. 4 for four different times ($t=0$, $T_0/4$, $T_0/2$, $3T_0/4$, with $T_0=1$ μs the period of the acoustical signal). The structure of the instantaneous amplitude is made of two lobes (a positive one—the white one—and a negative one—the black one) with the result that the amplitudes of two points, which are symmetric in relation to the center of the beam, have opposite signs. This is equivalent to the fact that the signals received at those two points have a difference of phase equal to π. The two lobes turn around the center of the beam. A rotation is accomplished for a period T. Note that the center of the beam is

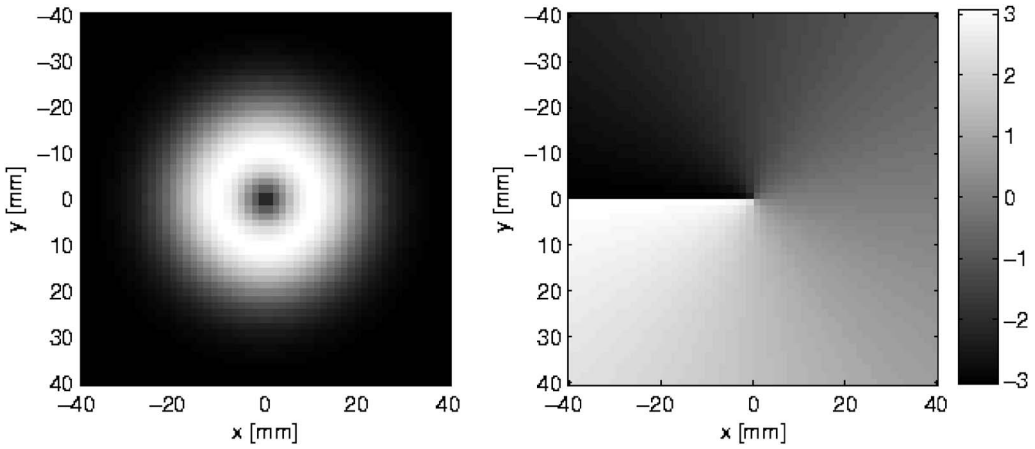

FIG. 3. Calculated amplitude rms and instantaneous phase of a perfect single vortex of charge −1.

always an area with a zero amplitude. To compare these results with those in optics, the rms amplitude is drawn in Fig. 5, where the well-known doughnut shape is recovered. The center of the beam exhibits a zero amplitude surrounded by a ring of constant amplitude due to the rotation of the two lobes. The size of the center at half depth is about 4.5λ. Therefore, the core of the beam is much thinner in acoustics than in optics where the typical width of the beam measured in controlled experiments is about 60λ. Indeed, optical vortices are observed in the far field of the source beyond the Rayleigh distance of the beam, contrarily to the experimental results obtained here. So, it is possible with the present experimental setup to investigate the behavior of the vortices from the near field to the far field. Another advantage of the acoustical techniques over the optical ones is the possibility of knowing accurately the phase of the beam. Indeed, the phase is measured directly and does not require one to solve an inverse problem or to compare the beam to a tilted one. Thus, the phase in the control plane (Fig. 5 on the right) can be compared to the phase prescribed in the pattern (Fig. 3 on the right). The similarity of the two images confirms that the measured beam possesses a screw dislocation as expected. The line of discontinuity is clearly visible (transition between white and black), the jump of 2π being particularly sharp. The helical structure is well recovered and points out the singularity at the extremity of the discontinuity line.

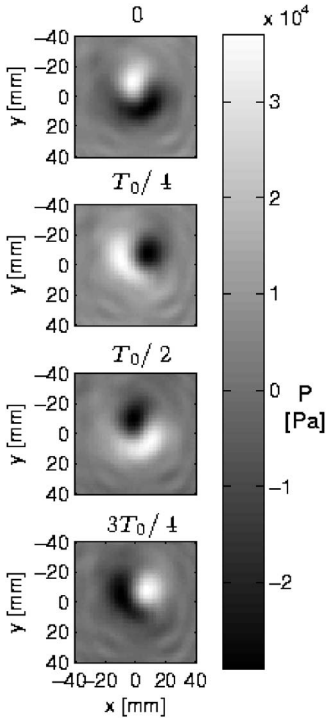

FIG. 4. Measured instantaneous amplitude for a vortex of charge 1 at four different times ($t=0, T_0/4, T_0/2, 3T_0/4$, with T_0 the period of the signal).

2. Single vortex of higher order

The experimental setup can synthesize single vortices of higher order just by applying a suitable pattern in the inverse filter phase. In a previous paper, it was shown that it could produce a single vortex of charge 2 [10]. But no attention was paid to its fine structure and its structural stability. In this paper, the capacity of the experimental setup to synthesize higher vortices is illustrated on a single vortex of charge −3 synthesized by two different methods: the first one consists in using the inverse filter technique and the second one consists in using the nonlinear parametric effect.

The GL mode $p_{3,-3}(r,\phi,0)$ with $w_0=10\lambda$ is taken as the pattern in the inverse filter technique. The rms amplitude and phase of that pattern are given in Fig. 6. The signals to emit by the array of transducers are calculated by the inverse filter technique and are emitted at low amplitude to ensure the linearity of the propagation. Then, the instantaneous amplitude is recorded at all points of the control plane. Figure 7 presents the instantaneous pressure for four different times: $t=0$, $T_0/4$, $T_0/2$, and $3T_0/4$. The pattern is made of six lobes: three positive ones and three negative ones, which are alternately located. We can clearly observe the rotation of the set of lobes around the center of the beam. Labeling the lobes (see the lobe labeled "1" in Fig. 7), it is possible to conclude that the complete rotation is achieved during one period. In this case, the rotation is clockwise in agreement with the sign of the topological charge. The representation of the rms amplitude plotted in Fig. 8 shows the classic circular shape already observed in optics, even if the amplitude struc-

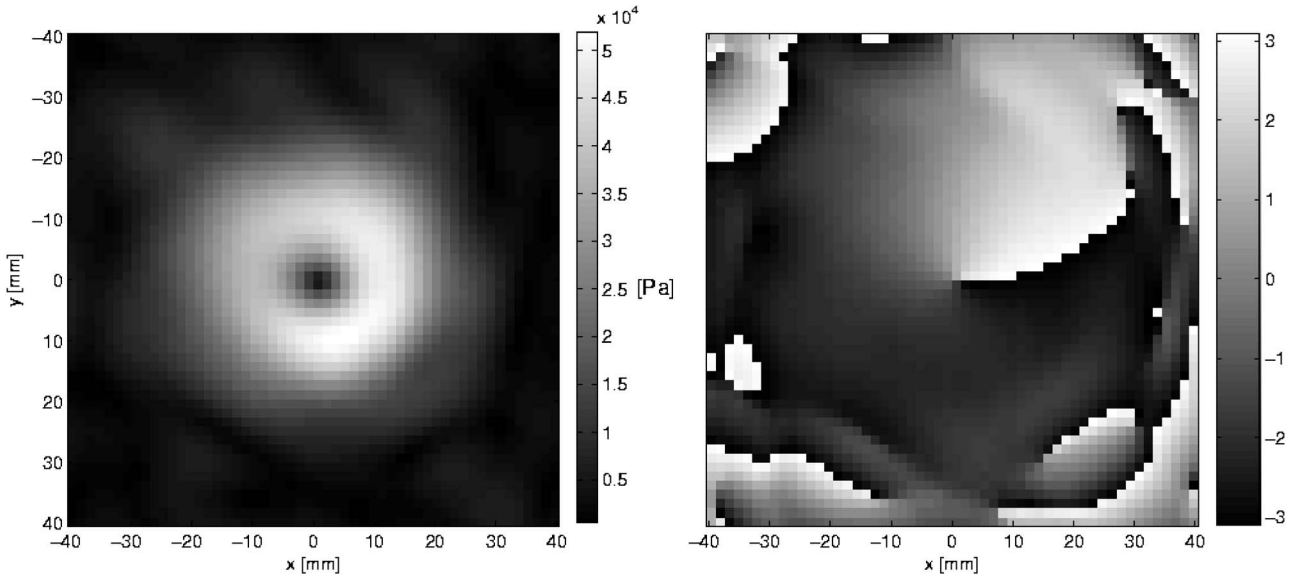

FIG. 5. Amplitude rms and instantaneous phase of the measured single vortex of charge −1.

ture is not a perfectly homogeneous ring. These defaults are due to the array of transducers used for the experiments. The structure of the phase (Fig. 8) is quite similar to those of the pattern (Fig. 6): the three lines of discontinuity (transition white-black) are well recovered but are not connected. This phenomenon is known as the instability of higher-order vortices [19]: a vortex of charge l is not stable and degenerates into $|l|$ vortices of charge $l/|l|$. It is discussed in the next section.

Another way to synthesize higher vortices is to use the parametric interaction which is a natural nonlinear effect in acoustics. If the amplitude of the waves is high enough, then nonlinear effects take place during the propagation and harmonics are generated. As water can be considered as a nondispersive medium, harmonics are traveling at the same speed. In a previous paper [10], it was demonstrated that if the medium is inviscid and isotropic, and if the nonlinear effects are weak, then the ratio between the topological charge and the number of the harmonic is constant. So, starting from a −1 vortex at frequency f_0, it is possible to produce a vortex of charge l in looking for the lth harmonic generated during the propagation. To illustrate that conservation law, the acoustical vortex of charge −1 described below has been reemitted with an amplitude ten times higher. Consequently, the propagation of this beam is no longer linear. Figure 9 shows the spectrum of the signal in the control plane. Starting from a signal emitted by the transducers with a frequency centered around $f_0=1$ MHz, we can clearly see that in the control plane the second, third, and fourth harmonics have been created and have a significant amplitude. Higher harmonics have also been detected up to 10 MHz but their amplitudes are weak. For each frequency of the spectrum, the corresponding phase pattern of the beam is plotted. The number of 2π jumps around the center of the beam increases linearly with the number of harmonics as theoretically predicted. As the medium is not dispersive, the beam is a superposition of vortices with different charges and different frequencies. As the wavelength associated with each vortex decreases linearly too, the domains on which the phase patterns are presented are smaller and smaller to keep the ratio

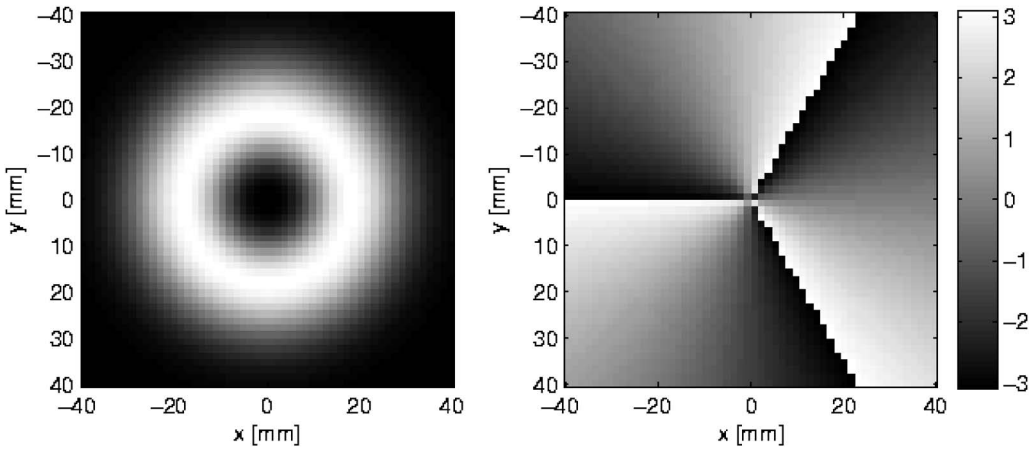

FIG. 6. Calculated amplitude rms and instantaneous phase of a perfect single vortex of charge −3.

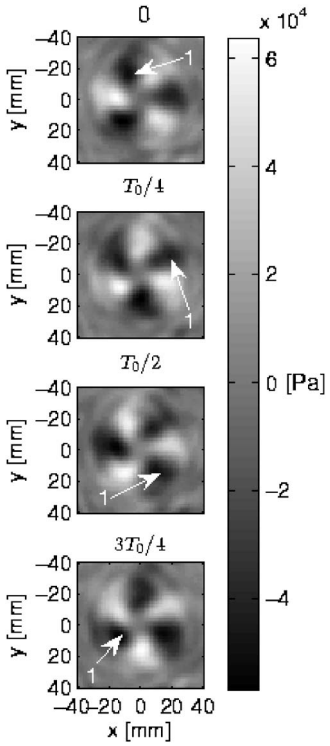

FIG. 7. Measured instantaneous amplitude of an acoustical vortex of charge −3 at four different times ($t=0, T_0/4, T_0/2, 3T_0/4$, with T_0 the period of the signal). The arrows indicate the positions of the lobe labelled "1."

of the extension of the domain to the wavelength constant. On each phase pattern, it is noticeable that the discontinuity lines are not exactly connected at the center: the screw dislocation of charge l is split into $|l|$ screw dislocations of charge −1. Again, this is related to the phenomenon of instability of the higher vortices discussed in the next section.

B. Modal analysis and localization of acoustical vortices

The experimental results show that the lines of phase discontinuity are not connected for vortices of charge greater than unity. In order to study accurately this phenomenon a modal decomposition has been performed. The Gauss-Laguerre modes are not only solutions of the paraxial equation but also have the important property of being a basis onto which it is possible to project any beam [17]. So it is possible to decompose any beam into GL modes and consequently it is possible to know precisely which of the modes make the beam.

The instantaneous amplitude of the pressure in any point of the measurement plane can be written $C_i(t)$, where i indexes the point of the measurement plane (for the presented experimental results $i \in [1:2916]$). In the linear regime, the signals are monochromatic, so it is more convenient to work at the fundamental frequency f_0 of the acoustic waves. Therefore, the Fourier transform of the temporal signal is performed and only the component at frequency f_0 is kept. This set of values can be arranged in a column vector $\hat{C}_i$. Considering the fact that the GL modes are an orthogonal basis, the field $\hat{C}_i$ can be projected onto this basis:

$$\hat{C}_i = \sum_{n,l} \hat{\alpha}_{l,n} p^i_{n,l}, \tag{7}$$

where $p^i_{n,l}$ is the GL mode with topological charge l and radial index n at the point indexed i and $\hat{\alpha}_{l,n}$ is the coefficients of the GL modes (n,l). As the measurements $\hat{C}_i$ have the dimension of a pressure and the GL mode $p_{n,l}$ is dimensionless, the coefficients $\hat{\alpha}_{l,n}$ have the dimension of a pressure. The problem can be expressed with the matrix form

$$\hat{\mathbf{C}} = \mathbf{B}\hat{\mathbf{A}}, \tag{8}$$

where $\hat{\mathbf{A}}$ is the vector containing the coefficients of projection on the GL basis, and $\mathbf{B}$ is a matrix $L \times N$ containing each GL mode $[-(L-1)/2 \leqslant l \leqslant (L-1)/2$ where L (an odd integer) is the maximum order of considered topological charge in the GL basis, and $n=\{|l|, |l|+2, \ldots, |l|+2(N-1)\}$ with N the maximum order of the considered radial index in the GL basis] on each control point i computed from Eq. (2).

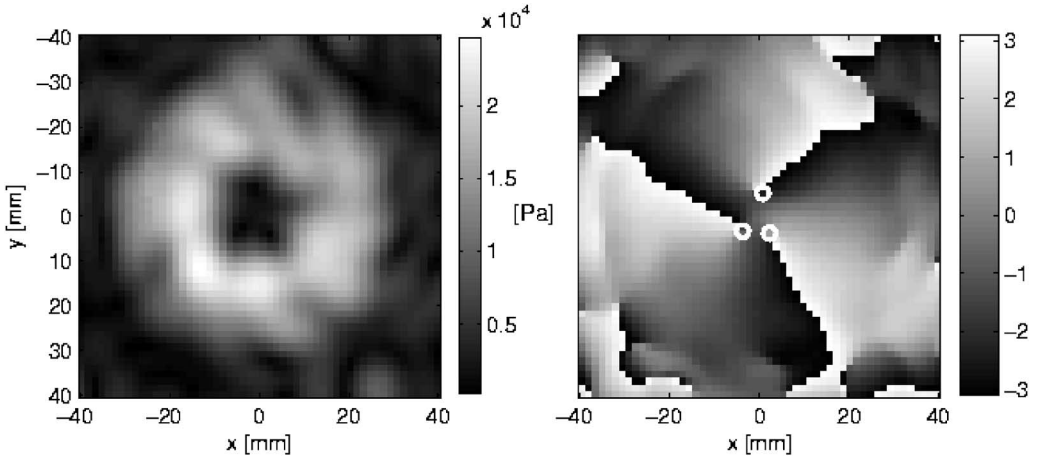

FIG. 8. Measured amplitude rms and instantaneous phase of a single vortex of charge −3 synthesized by inverse filter. White circles indicate the positions of the different acoustical vortices.

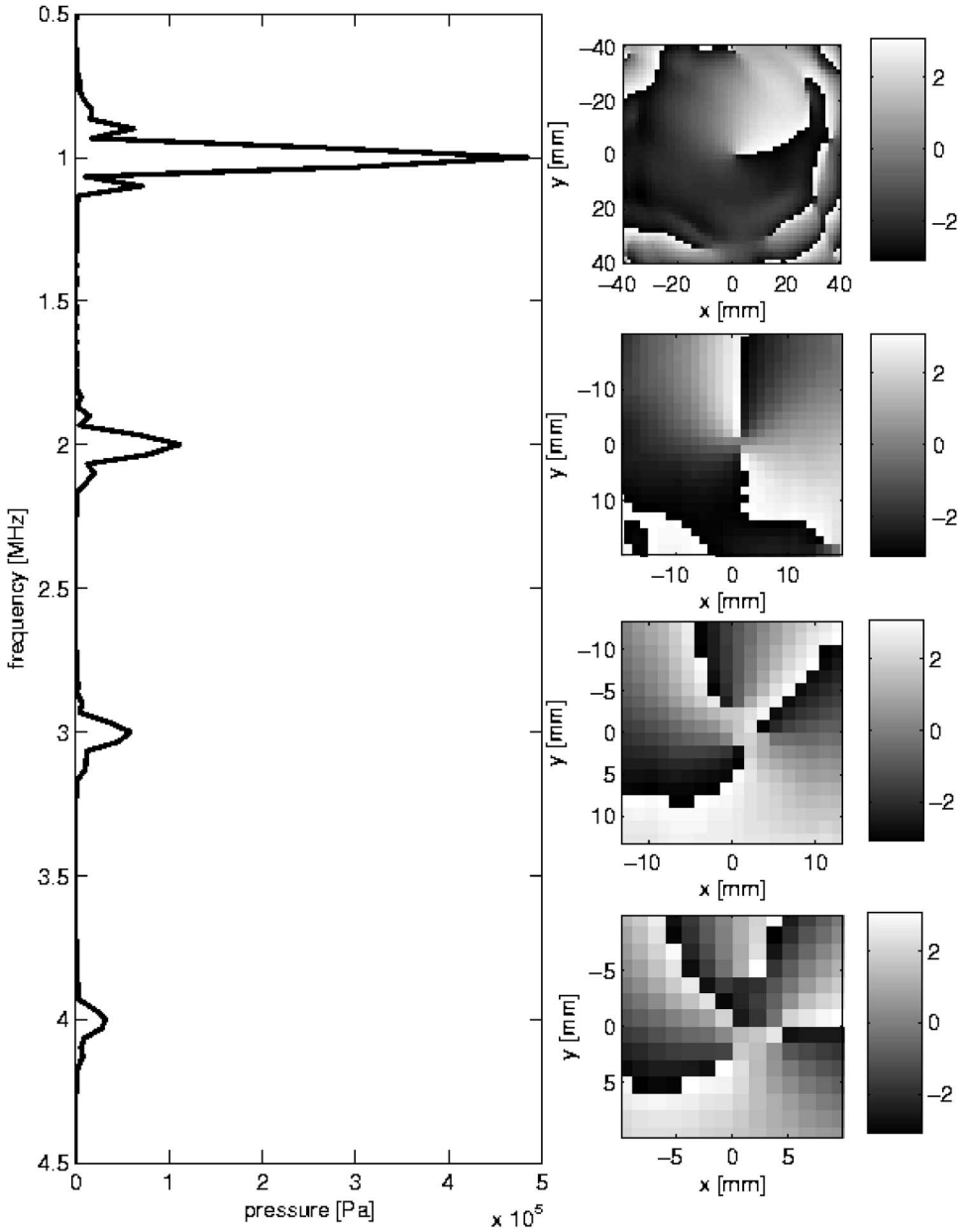

FIG. 9. Spectrum of the signal measured in the control plane (on the left) and phase (right) for the four first harmonics.

A GL analysis of vector $\hat{\mathbf{C}}$ consists in calculating all the coefficients $\hat{\alpha}_{l,n}$. That is possible by inversing the previous relation [(Eq. (8))]:

$$\hat{\mathbf{A}} = \mathbf{B}^{-1}\hat{\mathbf{C}}, \tag{9}$$

Note that, as matrix $\mathbf{B}$ is not square, the pseudoinverse technique is used to compute $\mathbf{B}^{-1}$.

Therefore it is possible to analyze the structure of a beam, and even an experimental one, in terms of GL modes. The required condition is to possess the instantaneous amplitude of each point of the control plane. Unlike optics for which the measurable quantity is the intensity, in acoustics this condition is satisfied. Hence, the modal decomposition of the experimental beams is computable. Figure 10 shows the modulus of coefficients $\hat{\alpha}_{l,n}$ determined by the GL analysis applied on the experimental single acoustical vortex of charge −1 presented in Sec. III A 1. The modulus of the coefficients is coded in gray level; the position on the grid indicates the considered mode (l,n) with l the topological charge and $n=|l|,|l|+2,\ldots$ the radial index. It is clear that the main contribution is due to the mode $l=-1$ and $n=|l|=1$. Nevertheless, the GL analysis shows that there exist several other contributions but one order of magnitude smaller than the main one. These contributions could be inherent to the experimental method. Indeed, the inverse filter method technique permits one to synthesize the closest field from the pattern in the sense of least squares. That means that the synthesized field could be slightly different from the prescribed one. Nevertheless, this explanation is not sufficient and the presence of other contributions must be interpreted carefully.

It is important to understand that the projection coefficients do not give access directly to the topological charge carried by the beam. Consequently, the results shown in Fig.

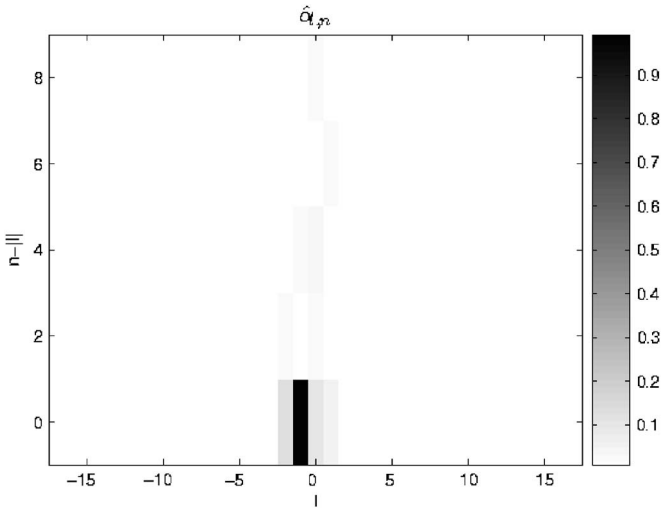

FIG. 10. Coefficients $\hat{\alpha}_{l,n}$ of the GL analysis for the experimental −1 vortex.

10 do not break down the conservation law of the topological charge even if modes with a charge different from −1 are in the projection. Projection coefficients indicate only the different modes needed to build the field as a sum of GL modes perfectly centered at the origin of the grid. The GL analysis of a perfect acoustical vortex (i.e., purely numerical) centered on the centre of the grid presented on Fig. 11 shows that the beam is composed only of a −1 vortex. But the GL analysis of the same beam with a center slightly different, for example located in $X_0=\lambda$ and $Y_0=0$, is not the same as illustrated in Fig. 11(b). However, these two beams are the same and, in particular, have the same topological charge. It is possible to calculate the topological charge from the coefficients of the GL analysis. According to Eq. (7), the field rebuilt from the coefficients of the GL analysis, denoted $\tilde{P}$ is

$$\tilde{P}(r,\phi,z)=\sum_{n,l}\hat{\alpha}_{l,n}p_{n,l}(r,\phi,z). \tag{10}$$

Note that the comparison between the rebuilt field $\tilde{P}$ and the measured one P permits to check the validity of the GL decomposition. The decomposition of the −1 vortex presented in Fig. 10 allows one to rebuild a field $\tilde{P}$ whose maximum difference of amplitude from the experimental one is always less than 0.1: $\max(|\tilde{P}-P|)\leqslant 0.1$.

The rebuilt field Eq. (10) can be expressed as a polynomial of the variable $e^{i\phi}$:

$$\tilde{P}(r,\phi,z)=e^{-[(L-1)/2]\phi}\sum_{\tilde{l}=0}^{L-1}\tilde{A}_{n,\tilde{l}}(r,z)e^{i\tilde{l}\phi}, \tag{11}$$

where $\tilde{l}=l+(L-1)/2$ takes only positive values and where the polynomial coefficients $\tilde{A}_{n,\tilde{l}}(r,z)$ are functions depending only on the variables r and z:

$$\tilde{A}_{n,\tilde{l}}(r,z)=\sum_{n}\hat{\alpha}_{\tilde{l},n}G(r,z)A_{n,\tilde{l}}(r,z)\Psi_n(z). \tag{12}$$

At a chosen distance $z=z_f$ (a fixed plane), and at a fixed radius $r=r_f$ from the axis of propagation, a vortex is characterized by a zero of amplitude $[\tilde{P}(r_f,\phi,z_f)=0]$ and a helical structure of the phase. Solving the polynomial

$$\sum_{\tilde{l}=0}^{L-1}\tilde{A}_{n,\tilde{l}}(r_f,z_f)X^{\tilde{l}}=0 \tag{13}$$

with $X=e^{i\phi}$ and searching only for roots such as $|X|=1$, we obtain the position of the vortices located at distance z_f and radius r_f. To detect all the vortices existing in the field, the whole radius r must be explored. The sum of the charges of all the detected vortices is, by definition, the topological

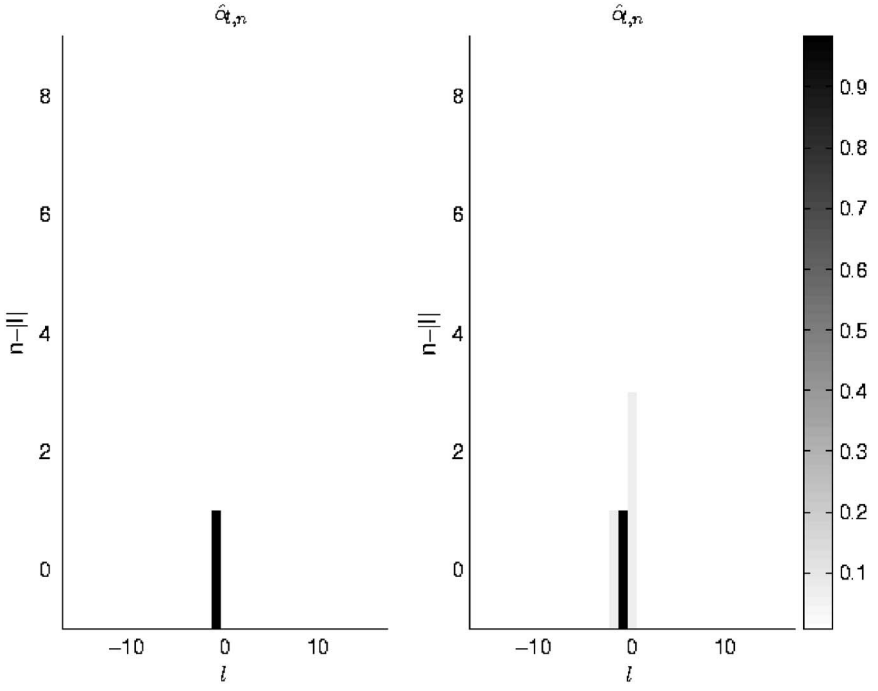

FIG. 11. Coefficients $\hat{\alpha}_{l,n}$ of the GL analysis for two perfect vortices with a −1 topological charge: (a) centered ($X_0=0$ and $Y_0=0$) and (b) decentered ($X_0=\lambda$ and $Y_0=0$).

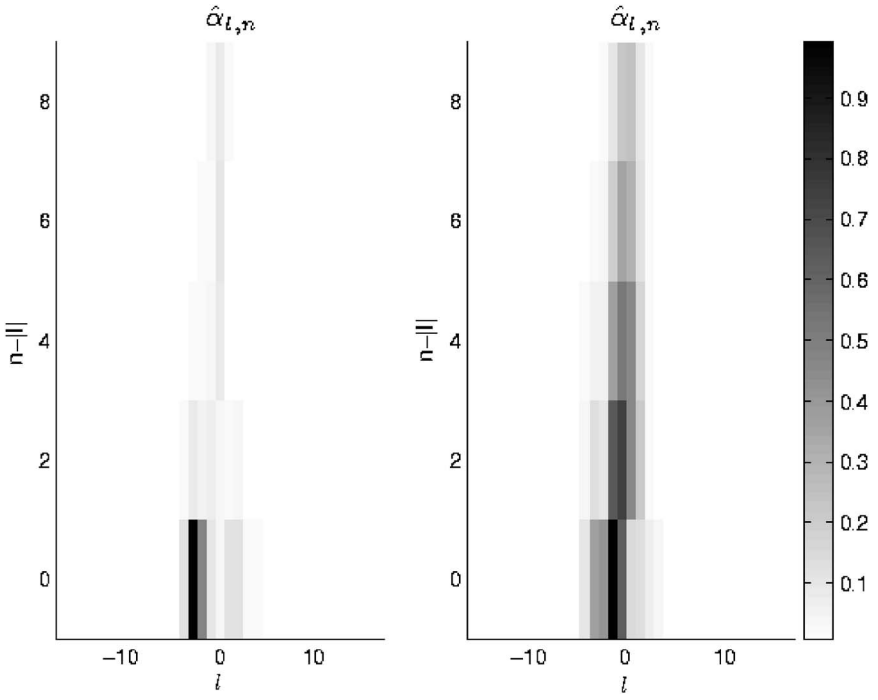

FIG. 12. Coefficients of the GL analysis for the experimental single −3 vortex and the experimental parametric −3 vortex.

charge of the beam. Thus, it is possible from the projection coefficients to determine precisely the position and the charge of all the screw dislocations contained in the field. The search for the roots of Eq. (13) is achieved numerically. It requires the introduction of a numerical parameter ϵ which is a tolerance on the modulus of the root. A root is considered as a vortex only if its modulus minus one is smaller than ϵ: $||X|-1|<\epsilon$. This is the only adjustable parameter introduced in this paper. Its value is currently chosen equal to 0.1. This technique applied to the −1 vortex presented above leads to one root located at $x=0.75$, $y=0.75$, the experimental step being $\Delta x=\Delta y=1.5$ mm. That means the field contains only one screw dislocation. Consequently, even if inherent weak pertubations propagate with the screw dislocation, the synthesis of a single −1 vortex is achieved. This property is related to the structural stability of the vortex with a unity charge [1]. That property strengthens the Hefner and Marston idea [8] to use acoustical vortices for underwater alignement.

It is interesting to apply the modal analysis and the localization technique to higher-order vortices. The GL analysis of the vortex of charge −3 synthesized by the inverse filter technique presented in Fig. 12 shows that the measured field is essentially a vortex of charge −3 but there exist other contributions which are more important than for the previous case. The localization procedure indicates that there exist three distinct roots localized at ($x=0.75$ mm, $y=-5.25$ mm), ($x=-3.75$ mm, $y=3.75$ mm), and ($x=2.25$ mm, $y=3.75$ mm). These coordinates correspond exactly to the end of the three different branches viewable in Fig. 8 and correspond to the white circles. So the beam is not made of one vortex of charge −3 as prescribed but of three vortices each of charge −1. But that kind of structure with $|l|>1$ is expected to be structurally unstable [1], so that any weak perturbation would degrade a vortex of charge $|l|$ into $|l|$ vortices of charge $|1|$. The consequences are that the discontinuity lines are disconnected and there exist three separated zeros of amplitude in Fig. 8. It is important to outline that the concept of stability invoked to explain this phenomenon is related to structural stability in the sense of catastrophe theory [20] rather than the usual stability of hydrodynamics. This is related to the structural instability of a perfect focus point which degenerates into stable caustics.

In the case of the single vortex of charge −3 produced by parametric interaction, the situation is analoguous. The GL analysis presented in Fig. 12 shows that the main contribution is due to the −2 GL mode but there also exist other modes which have important contributions. That result emphasizes that the information contained in the GL analysis is not directly the topological charge. The important number of different modes explains the splitting of the discontinuity lines. The localization procedure indicates that there exist three different roots localized at ($x=0.75$ mm, $y=-2.25$ mm), ($x=3.75$ mm, $y=0.75$ mm), and ($x=-0.75$ mm, $y=0.75$ mm). The fact that the discontinuity lines are closer to the center is mainly due to the frequency of the beam which is here $3f_0$. So the spatial scale is smaller. It is noticeable than the −3 vortex is broken even in this case because the parametric generation implies a continuous creation of that mode from the lower modes. This situation outlines the concept of structural instability invoked to explain the behavior of higher vortices. The least perturbation provokes a splitting of a higher vortex into single vortices with conservation of the total topological charge if the medium is isotropic and inviscid.

C. Interaction of two vortices with the same or opposite charges

Patterns with several acoustical vortices can be synthesized directly with the versatile experimental setup. Because

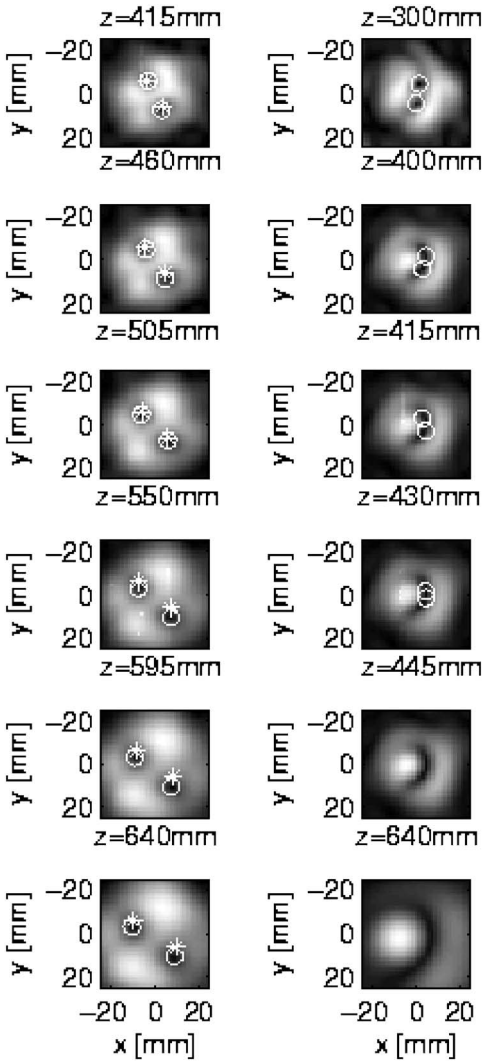

FIG. 13. Measured amplitude rms of two vortices with same charge on the left and with opposite charge on the right. The circles denote the positions of the screw dislocations located by the method of localization explained below. The stars show the theoretical positions of the screw dislocations for two vortices with same charge according to Eqs. (14) and (15).

of analogies with hydrodynamics or quantum mechanics, the interactions between several screw dislocations present great interest. The number of vortices and their charge could be theoretically chosen arbitrarly. The main restriction is due to the aperture and definition of the array of transducers. In this paper, a study about interactions between two vortices of the same and opposite charge is presented. For both cases, the vortex cores are separated by 12λ and they are nested in a Gaussian beam of 10λ width. The control plane is located 30 cm away from the array of transducers. Only the charges of the two vortices are different: in the first case the two vortices are equally charged ($l_1=l_2=-1$) and in the second case, the charges of the vortices are opposed ($l_1=-1$ and $l_2=1$). The evolution of the two vortices with the same charge is presented in Fig. 13 on the left column. Measured rms amplitudes at six different planes located at $z=415$, 460, 505, 550, 595, and 640 mm away from the transducers are presented. The measured pressure is coded in gray level; circles show the positions of the screw dislocation detected by the GL analysis associated with the localization method. The stars indicate the theoretical position of the screw dislocations. The two cores remains symmetric in relation to the center. They are rotating counterclockwise. The distance between them is increasing with the propagation distance. This behavior can be compared to the behavior theoretically predicted by Indebetouw [21] and numerically checked by Rozas *et al.* [22]. They show that, in a plane z, the positions of the vortices, denoted in cylindrical coordinates by $R_j(z)$ and $\Theta_j(z)$ with $j\in\{1,2\}$, are described by

$$R_j(z) = R_j(0)(1 + z^2/Z_R^2)^{1/2} \tag{14}$$

and

$$\Theta_j(z) = \Theta_j(0) - \mathrm{sgn}(m)\arctan(z/z_R), \tag{15}$$

where $j\in\{1,2\}$, and $R_j(0)$ and $\Theta_j(0)$ is the center of the jth vortex in the plane $z=0$. The positions of the vortices are calculated by using the prescribed positions for the two vortex in $z=300$ mm, namely, $(R_1(0)=6\ \mathrm{mm}, \Theta_1(0)=\pi)$ and $(R_2(0)=6\ \mathrm{mm}, \Theta_1(0)=0)$. The theoretical positions are the stars plotted on the left column of Fig. 13. We can see that the agreement between the theoretical law and the experimental results is very good. According to [21], that comparison shows that on the considered propagation domain, the two vortices move away on parallel straight lines. There are no interactions between the two vortices, unlike the fluidlike motion observed for point vortices in optics [22].

The evolution of two vortices with opposite charges is presented in the right column of Fig. 13. The field has been measured in different transverse planes located at $z=300$, 400, 415, 430, 445, and 640. The circles show the positions of the screw dislocations detected with the localization method described below. The first picture (at $z=300$ mm) measured in the control plane shows a field close to the fields presented in the left columns: we can see two cores nested in a Gaussian spot. Nevertheless, during the propagation, the behavior of this beam is radically different from the previous one. Indeed, we can see clearly that the two vortices are closer and closer until their merging. The method of localization indicates that there exist two screw dislocations from $z=300$ to 430 mm; after that distance, no screw dislocations are detected. Note that this behavior does not break the law of conservation of the topological charge. Indeed, the inital pattern contained two screw dislocations with opposite charge, so the total topological charge is zero as after the merging of the two vortices.

IV. CONCLUSIONS AND OUTLOOK

Thanks to the versatility of the experimental setup, several configurations of acoustical vortices were realized experimentally as single acoustical vortices of higher order and interactions of two acoustical vortices. The features of acoustics allowed us to measure instantaneous pressure and phase and so permitted us to perform a GL analysis of the experimental beams. This decomposition associated with our local-

ization method allows us to determine accurately the position of the screw dislocation in an acoustical field. In particular, the positions of different single vortices created by the splitting of a higher vortex have been obtained. That result confirms the property of structural instability of the higher vortices. The structural stability of a single vortex has been observed too. For the interaction of two vortices, experimental results have been compared successfully to the theoretical law of evolution, proving that there is no interaction for two Gauss-Laguerre acoustical vortices. The localization method has permitted us to observe accurately the merging of two vortices with opposite charges. The theoretical and experimental basis for acoustical vortices seems to be solid enough to envisage the next step. Acoustical spanners are very attractive because of their potential applications to manipulate small objects. Moreover, the real time control of the field is a reasonnable improvement of this experimental setup as mentioned above. Another appealing subject is the possibility of creating acoustical solitons or solitary waves similar to the dark solitons in optics, for which nonlinear effects would compensate diffraction effects.

ACKNOWLEDGMENTS

The authors are very gratefull to F. Coulouvrat and M. Rossi [LMM, UPMC, and CNRS (UMR 7607, Paris)] for fruitful discussions about this paper.

[1] J. F. Nye, *Natural Focusing and Fine Structure of Light* (Institute of Physics Publishing, Bristol, 1999).
[2] W. Whewell, Philos. Trans. R. Soc. London **123**, 147 (1833).
[3] J. F. Nye and M. V. Berry, Proc. R. Soc. London, Ser. A **336**, 165 (1974).
[4] M. S. Soskin and M. V. Vasnetsov, Prog. Opt. **42**, 221 (2001).
[5] M. Mansuripur and E. M. Wright, Opt. Photonics News **1**, 40 (1999).
[6] L. Allen, M. W. Beijersbergen, R. J. C. Spreeuw, and J. P. Woerdman, Phys. Rev. A **45**, 8185 (1992).
[7] Z. Bouchal, J. Wagner, and M. Chlup, Opt. Commun. **151**, 207 (1998).
[8] B. T. Hefner and P. L. Marston, J. Acoust. Soc. Am. **106**, 3313 (1999).
[9] S. Gspan, S. Bernet, and M. Ritsch-Marte, J. Acoust. Soc. Am. **115**, 1142 (2004).
[10] J.-L. Thomas and R. Marchiano, Phys. Rev. Lett. **91**, 244302 (2003).
[11] B. Y. Zel'dovich, N. F. Pilipetskii, and V. V. Shkunov, *Principles of Phase Conjugation* (Springer, Berlin, 1985).
[12] V. Y. Bazhenov, M. S. Soskin, and M. V. Vasnetsov, J. Mod. Opt. **39**, 985 (1992).
[13] M. W. Beijersbergen, L. Allen, H. V. der Veen, and J. P. Woerdman, Opt. Commun. **96**, 123 (1993).
[14] S. N. Khonina, V. V. Kotlyar, M. V. Shinkaryev, V. A. Soifer, and G. V. Uspleniev, J. Mod. Opt. **39**, 1147 (1992).
[15] J. E. Curtis and D. G. Grier, Phys. Rev. Lett. **90**, 133901 (2003).
[16] M. Tanter, J.-L. Thomas, and M. Fink, J. Acoust. Soc. Am. **108**, 223 (2000).
[17] R. Piestun, Y. Y. Schechner, and J. Shamir, J. Opt. Soc. Am. A **17**, 294 (2000).
[18] *Handbook of Mathematical Functions*, edited by M. Abramowitz and I. Stegun (Dover, New York, 1965).
[19] I. V. Basistiy, V. Y. Bazhenov, M. S. Soskin, and M. V. Vasnetsov, Opt. Commun. **103**, 42 (1993).
[20] M. V. Berry, Adv. Phys. **25**, 1 (1976).
[21] G. Indebetouw, J. Mod. Opt. **40**, 73 (1993).
[22] D. Rozas, C. T. Law, and G. A. Swartzlander, J. Opt. Soc. Am. B **14**, 3054 (1997).